ELSEVIER

Polymer 43 (2002) 6727–6741

polymer

www.elsevier.com/locate/polymer

Thermal expansion behavior of nylon 6 nanocomposites

P.J. Yoon, T.D. Fornes, D.R. Paul*

Department of Chemical Engineering and Texas Materials Institute, The University of Texas at Austin, Austin, TX 78712, USA

Received 24 June 2002; received in revised form 29 August 2002; accepted 3 September 2002

Abstract

The linear thermal expansion behavior of nanocomposites was measured and compared with the theory by Chow. Nanocomposites were prepared by melt mixing organically modified montmorillonite with high and low molecular weight (LMW) grades of nylon 6 using a twin screw extruder. Thermal expansion measurements were made on samples taken from injection-molded Izod bars in the flow direction (FD), transverse direction (TD), and normal direction (ND). Addition of clay reduces the thermal expansion coefficient in both FD and TD while an increase is seen in ND; FD has a lower thermal expansion coefficient than TD. The latter suggests non-uniform orientation of exfoliated platelets about FD, since perfect alignment of disk-like platelets in an isotropic matrix must yield identical expansion coefficients for both FD and TD. High molecular weight (HMW) nylon 6 nanocomposites resulted in lower thermal expansion than LMW nylon 6 nanocomposites at the same organoclay content. This difference was attributed to the higher aspect ratio of particles (better exfoliation) in HMW nylon 6 nanocomposites. Thermal expansion coefficients predicted from a theoretical composite model were compared to the experimental data. Platelet aspect ratios deduced in this way were found to be dependent on the specimen direction, which further suggests imperfect orientation of particles about FD. Morphological analysis by transmission electron microscopy support the conclusions drawn above.

Keywords: Nylon 6; Nanocomposites; Linear thermal expansion coefficient

1. Introduction

Polymer layered silicate nanocomposites potentially offer higher stiffness and strength [1,2], gas barrier properties [3,4], dimensional stability [1,5,6], and other attractive physical properties. Recent studies have shown that these benefits can be achieved by melt processing, for some polymer matrices, provided the structure of the organoclay and processing conditions are properly chosen [7–10].

One important advantage of such nanocomposites over conventional composites is that less filler is needed to achieve a given level of reinforcement which leads to weight savings in structural parts. For example, nylon 6 nanocomposites containing only 4 wt% of well-exfoliated silicate layers can yield mechanical properties or dimensional stability comparable to a conventional nylon 6 composite containing 20 wt% mica [11]. These advantages are believed to stem from the high aspect ratio and high modulus of the silicate platelets. Another inherent advantage of nanocomposites for such applications is the potentially better surface finish that can be achieved relative to commercial composites owing to the much smaller size of the filler phase. Nanocomposites have been formed by various techniques such as in situ polymerization [1,3,4,11], sol–gel templating [12], and melt compounding [5,7–10]. Recent reports about automotive applications have emphasized that melt processing plays a pivotal role in the development of commercially viable materials [13,14].

A major issue for polymers in engineering applications is to reduce the thermal expansion coefficient to achieve dimensional stability more comparable to metals. Numerous studies have examined how filler shape, size, and volume fraction influence the thermal expansion of polymer composites. Long fiber composites have a significantly lower linear thermal expansion coefficient than the matrix polymer [15]. Polymer nanocomposites are also expected to have improved thermal expansion properties; however, few experimental data are currently available. The Toyota research group observed anisotropic thermal expansion behavior for injection-molded specimens; the expansion coefficient in the flow direction (FD) was lower than in the

* Corresponding author. Tel.: +1-512-471-5392; fax: +1-512-471-0542.
E-mail address: drp@che.utexas.edu (D.R. Paul).

0032-3861/02/$ - see front matter
PII: S0032-3861(02)00638-9

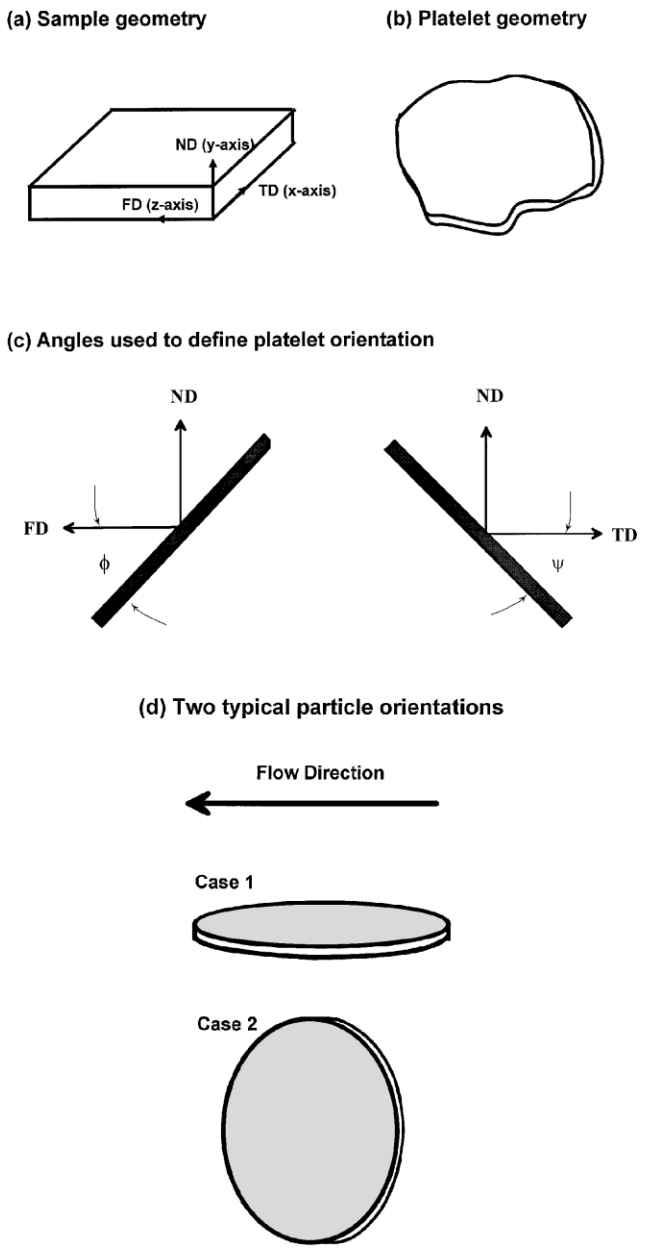

Fig. 1. Illustrations of (a) sample geometry, (b) platelet geometry, (c) platelet orientation to define orientation angle, and (d) two typical cases of particle orientation.

perpendicular direction [16,17]. However, the effects of clay orientation, matrix–clay interaction, and processing techniques on thermal expansion are not fully understood.

The purpose of this paper is to document the thermal expansion behavior of nanocomposites prepared from organically modified montmorillonite and nylon 6 using melt processing. Emphasis is placed on how the concentration, orientation, and level of exfoliation of the clay platelets influence expansion behavior for injection-molded specimens. Transmission electron microscopy (TEM) is employed to elucidate platelet orientation in the three principle directions of the injection-molded bar. In addition, the theoretical model by Chow [18,19] is used to predict thermal expansion behavior. The model is unique in that it considers the filler aspect ratio, unlike other thermal expansion models available in the literature [20–23]. Finally, it is important to note that nylon 6, being a semi-crystalline polymer, may exhibit different levels of thermal expansion due to changes in the crystalline phase (e.g. level of crystallinity, crystallite size, shape, type, and orientation). Studies have shown that the addition of dispersed silicate platelets influences the crystalline characteristics of nylon 6 [24,25]. To fully understand how such changes in the nylon 6 matrix caused by the addition and dispersion of montmorillonite affect the thermal expansion behavior of the nanocomposite is extremely difficult and beyond the scope of this work. The primary goal here is to report the thermal expansion behavior of various nylon 6 nanocomposites obtained by melt processing. This work is part of a continuing investigation of melt processed nanocomposites; the materials used in this work have been described previously [9,10].

2. Background

The physical properties of injection-molded specimens are known to depend on direction within the specimen relative to the flows involved in its formation. Processing directions are commonly described by an orthogonal coordinate system identified by the flow direction (FD), transverse direction (TD), and normal direction (ND) as defined in Fig. 1(a). This nomenclature is used throughout the remainder of this paper. The properties of injection-molded polymer nanocomposites are expected to be sensitive to direction, especially when the high aspect ratio, aluminosilicate platelets are individually dispersed in the polymer. Dispersed platelets are expected to resemble disks, as shown in Fig. 1(b). Depending on the flow fields encountered during injection molding, these platelets may have a wide range of orientations within the polymer matrix. The orientation of the platelets with respect to the three orthogonal principle directions can be described as shown in Fig. 1(c). The angles ϕ and ψ indicate the orientation of a platelet with respect to FD and TD, respectively.

The linear thermal expansion of a nanocomposite will greatly depend on the average orientation of the platelets and is expected to follow the trends listed in Table 1 if we assume that any anisotropy of the matrix itself induced by the filler is of secondary importance. Consider two extreme cases; viz. the surfaces of platelets are parallel to FD and to TD (*case 1*) or to the ND (*case 2*). For either orientation, the thermal expansion in FD will be the same and have the maximum reduction from that of the matrix due to the constraining effect of the inorganic filler; however, thermal expansion in the TD or the ND will depend on platelet orientation about the FD axis. If all the platelets are arranged as in case 1, then linear expansion coefficients (LECs) in the flow and the TD should be identical if the filler particles can

Table 1
Effect of particle orientation on the linear thermal expansion coefficients

For this orientation	Expected result
$\langle\phi\rangle = 0$; $\langle\psi\rangle = 0°$ (case 1)	$\alpha_{ND} > \alpha_{FD} = \alpha_{TD}$
$\langle\phi\rangle = 0$; $\langle\psi\rangle = 90°$ (case 2)	$\alpha_{ND} = \alpha_{FD} < \alpha_{TD}$
$\langle\phi\rangle = 0$; $\langle\psi\rangle = 45°$ (or random)	$\alpha_{FD} < \alpha_{ND} = \alpha_{TD}$
$\langle\phi\rangle \sim 0$; $0° < \langle\psi\rangle < 45°$	$\alpha_{ND} > \alpha_{TD} > \alpha_{FD}$
$\langle\phi\rangle \sim 0$; $45° < \langle\psi\rangle < 90°$	$\alpha_{TD} > \alpha_{ND} > \alpha_{FD}$

be considered as squares or disks. However, when a significant fraction of the platelets are arranged as in case 2, then the LEC in the TD should be larger than in FD because the filler cannot constrain the linear thermal expansion of the matrix to the same extent. Therefore, the details of platelet orientation must be carefully considered to understand the thermal expansion behavior of nanocomposites.

There have been many studies on how anisotropic particles align during flow [26–29]. For example, it has been shown that the plate-like particles of kaolinite suspended in D_2O develop a high degree of FD orientation in Poiseuille flow [26]. Numerical methods have been used to study the dynamics of plate-like particle orientation in simple shear flow [27]. It was predicted that planar orientation of the particles should occur in the shear direction with the major axis of rectangular plates aligned in the direction of shear. The shear orientation of a clay–polymer solution was also studied using rheological and flow birefringence techniques [28]. Birefringence showed a minimum with increasing steady shear rate, suggesting that clay particles orient first, while polymer chains begin to orient at a critical shear rate.

The effect of inorganic filler orientation on the reduction of linear thermal expansion is similar to the effect on modulus enhancement or reinforcement which has been studied more extensively. Brune and Bicerano [29] have shown by numerical methods that the extent of reinforcement in composites can be significantly decreased by small off-plane deviations from perfect in-plane orientation; this effect is particularly pronounced for platelets of high aspect ratio.

Filler geometry can also greatly affect physical properties of composites; e.g. high aspect ratios contribute to greater reduction in thermal expansion [30] and greater increase in modulus [9]. A recent study of melt compounded nylon 6/organoclay nanocomposites showed that the extent of exfoliation and subsequently the aspect ratio of the filler phase are significantly improved by higher shear stresses in the extruder. Nanocomposites based on a high molecular weight (HMW) nylon 6 showed greater reinforcement (modulus increase) in both the melt and solid-state than those based on a low molecular weight (LMW) nylon 6; this was attributed to the higher melt viscosity and, hence, higher stresses experienced during processing. TEM images of the HMW nylon 6 nanocomposites showed well-exfoliated structures while the LMW nylon 6 nanocomposites showed less exfoliation. A quantitative analysis of the TEM images for HMW and LMW nylon 6 nanocomposites revealed a higher number of particles per (μm^2 and fewer platelets per particle for the HMW composites as compared to the nanocomposite based on LMW nylon 6. These differences in number and final shape of the dispersed particles between the two polyamides should yield differences in thermal expansion behavior.

Fillers typically have significantly higher moduli and sizably lower expansion coefficients than most polymer matrices; these differences are even more pronounced above the polymer's glass transition temperature (T_g). Enhancement of dimensional stability is expected when a filler with high modulus and low thermal expansion coefficient is dispersed in a matrix of lower modulus and higher thermal expansion coefficient owing to simple mechanical restraints. Glass fibers are commonly added to polymer matrices for this purpose in addition to increasing stiffness. Layered silicates seem attractive for this purpose owing to their high modulus, high aspect ratio, and low coefficient of thermal expansion; in addition, they are likely to be less detrimental to surface finish and ductility than conventional fillers.

Finally, it should be mentioned that the matrix material in this case can be considered as a composite consisting of both amorphous and crystalline phases. Since these two phases may have significantly different properties, variations in crystalline type, orientation, size, and quantity will affect the properties of the matrix and, hence, composites are made from it. Then, some of the property responses of nylon 6-based nanocomposites may stem from changes in the matrix caused by the presence of the filler; however, this should be a second-order effect compared to the direct effects of filler on the composite performance as predicted by appropriate composite theories.

3. Experimental

3.1. Materials

Two commercial nylon 6 materials were chosen for this study (Table 2) that represent low and high molecular weight grades referred to here as LMW and HMW. The organoclay, supplied by Southern Clay Products, Inc., was formed by a cation exchange reaction between sodium montmorillonite (CEC = 92 mequiv./100 g clay) and bis(hydroxyethyl)-(methyl)-rapeseed quaternary ammonium chloride, designated here as $(HE)_2M_1R_1$. All data below are reported in terms of the weight percent montmorillonite (MMT) in the composite rather than the amount of organoclay, since the silicate is the reinforcing component.

Table 2
Materials used in this study

Material (designation used here)	Supplier designation	Specifications	Supplier
Nylon 6 (LMW)	Capron 8202	$\bar{M}_n = 16\,400$[a]	Honeywell (formerly AlliedSignal)
Nylon 6 (HMW)	Capron B135WP	$\bar{M}_n = 29\,300$[a]	Honeywell (formerly AlliedSignal)
Organoclay $[(HE)_2M_1R_1]$	Bis(hydroxyethyl)-(methyl)-rapeseed quaternary ammonium organoclay	Organic loading = 95 mequiv./100 g clay, organic content = 34.6 wt%	Southern Clay Products

[a] $\bar{M}_n$ determined via intrinsic viscosity using *m*-cresol at 25 °C [31].

3.2. Melt processing

Melt blended composites were prepared using a Haake, corotating, intermeshing twin screw extruder (diameter = 30 mm, $L/D = 10$). Compounding was carried out at a barrel temperature of 240 °C, a screw speed of 280 rpm, and a feed rate of 980 g/h. Polyamide materials were dried in a vacuum oven at 80 °C for a minimum of 16 h while the organoclay was used as received.

Izod specimens (ASTM D256) were prepared by injection-molding using an Arburg Allrounder 305-210-700 injection molding machine. Test specimens were prepared using a barrel temperature of 260 °C, mold temperature of 80 °C, injection pressure of 70 bar, and a holding pressure of 35 bar. After molding, the specimens were immediately sealed in a polyethylene bag and placed in a vacuum desiccator for a minimum of 24 h prior to thermal expansion testing.

3.3. Thermal expansion measurement

Thermal expansion tests were conducted according to ASTM D696 using a Perkin–Elmer thermomechanical analyzer (TMA 7). Rectangular specimens were prepared by milling the center part of injection-molded Izod bars (as-molded) to the following dimensions: 3.175 mm thickness, 6.35 mm width, and 12.7 mm height. To investigate the directional dependence of thermal expansion, measurements were made in the three orthogonal directions, i.e. FD, TD, and ND, as depicted in Fig. 1. The thermal expansion in ND was measured by stacking two specimens together to provide the needed minimum height. In order to examine the effect of the thermal history, specimens were annealed at 150 °C for 8 h in a vacuum oven (*annealed*). Thermal expansion tests were performed over the temperature range from −10 to 150 °C at the rate of 5 °C/min in a nitrogen atmosphere.

3.4. Electron microscopy

Samples for TEM analysis were taken from the core portion of an Izod bar parallel to the three orthogonal axes (Fig. 1) in order to assess silicate platelet orientation and anisotropy. Ultrathin sections approximately 50 nm in thickness were cryogenically cut with a diamond knife at a temperature of −40 °C using a Reichert-Jung Ultracut E microtome. Sections were collected on 300 mesh gold grids and subsequently dried with filter paper. The sections were examined by TEM at an accelerating voltage of 120 kV using a JOEL 2010F TEM equipped with a field emission gun. Selected images were analyzed for particle size to determine the degree of platelet anisotropy. TEM images were printed on $20.3 \times 25.4\ cm^2$ photographic paper. A transparent plastic sheet was placed over the print and dispersed platelets and/or agglomerates were traced over using a black permanent pen. The resulting image was electronically scanned and subsequently analyzed using an image analysis program (NIH® Image software, Scion Image).

In addition to TEM analysis, selected sections were viewed on the same electron microscope via scanning transmission electron microscopy (STEM) in the high angle annular dark field (HAADF) mode. STEM observations were conducted using an accelerating voltage of 200 kV and a camera length of 30 cm.

4. TEM/STEM analysis

Fig. 2 shows photomicrographs of nanocomposites sections taken from the core region of injection-molded test specimen as viewed parallel to the three orthogonal axes, FD, TD, and ND axes shown in Fig. 1. Fig. 2(a) shows a well-exfoliated system of dispersed silicate platelets within the HMW nylon 6 matrix as viewed parallel to FD. The majority of the platelets appear to be edge-on, with only a small fraction of visible skewed faces. Skewed or tilted faces often appear as medium to dark shades of gray bordering a silicate platelet edge. The platelets are somewhat random, showing some preferential alignment parallel to TD. Fig. 2(a′) reveals similar orientation effects for the equivalent LMW nanocomposite, however, at a lower degree of silicate platelet exfoliation. The LWM system consists of regions of dispersed singlets, doublets, and triplets, and regions of intercalated platelet stacks. The number of particles per unit area, or particle density, is considerably lower for the LMW based nanocomposite. The larger distances between particles are a further indicator of less silicate platelet exfoliation as compared to the HMW nanocomposite image. With regard to platelet orientation

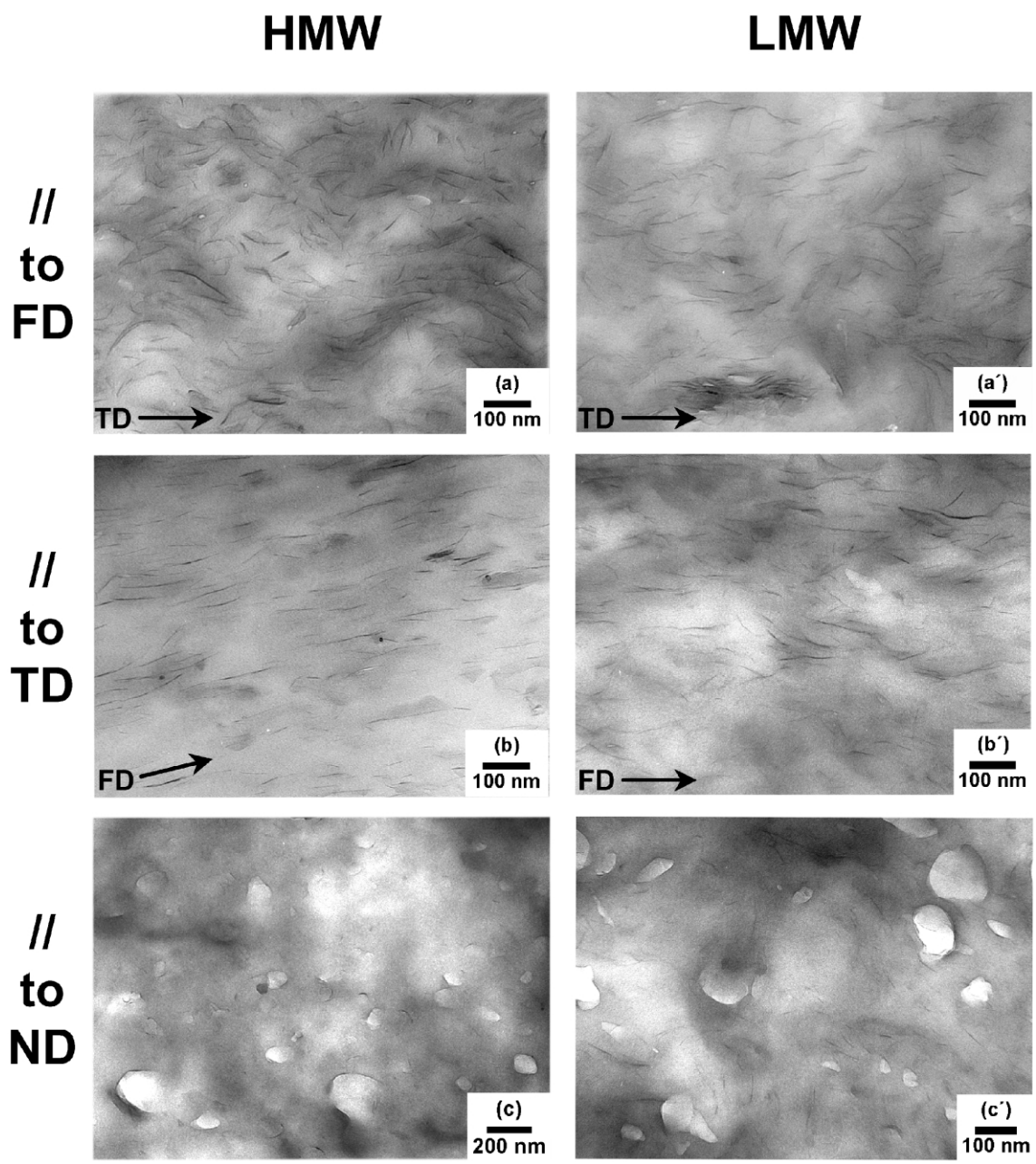

Fig. 2. TEM photomicrographs of nanocomposites based on HMW and LMW nylon 6 taken from the core region of injection-molded specimens viewed parallel to the flow (a, a′), transverse (b, b′), and normal (c, c′) directions.

platelets are primarily seen edge-on in the LMW image. Similar to the HMW system, the edges are somewhat random but have a general preference to align along the TD axis. It is worth noting that these observations agree with previously reported results [9,10].

Photomicrographs of sections viewed parallel to the TD axis are presented in Fig. 2(b) and (b′). The nanocomposite based on HMW nylon 6, Fig. 2(b), reveals exfoliated platelets, seen edge-on, that are well aligned along the FD. A significant number of tilted faces are visible throughout the photomicrograph. Presence of such faces is expected since some random orientation is observed in views parallel to the FD axis. The TEM image of the LMW composite, Fig. 2(b′), reveals a similar trend in which platelet edges dominate and are aligned largely along the FD axis. The degree of platelet alignment, however, appears to be less pronounced than in the HMW matrix. This difference may be attributed to two factors, a lower degree of platelet exfoliation and/or rheological differences. A system that is more exfoliated will have more exposed silicate surface than a partially exfoliated system. High aspect ratio, high surface area particles will be more prone to align in the polymer FD as compared to a less anisotropic stack of platelets. A lower degree of exfoliation for the LMW nanocomposite is also evident in this TD view, visible through a lower particle density and larger inter-particle

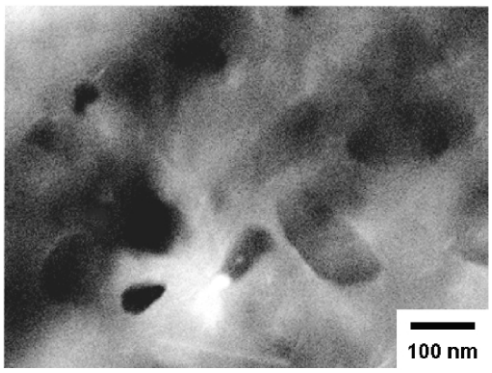

Fig. 3. HAADF STEM image of the nanocomposite based on LMW nylon 6 taken parallel to the ND axis.

distances compared to the HMW nanocomposite. Differences in the melt rheology between the two systems may also contribute to more or less pronounced platelet alignment. The higher molecular weight polyamide will impart higher shear stresses on the platelets, which may lead to more alignment along the FD.

TEM photomicrographs of sections viewed parallel to the ND axis are seen in Fig. 2(c) and (c′). Both photomicrographs exhibit a large fraction of light colored, round objects. Interestingly, their size and shape are of the same dimensions as silicate platelets. It was speculated that these objects may indeed be platelets or perhaps cavities associated with platelet pullout during the microtoming process. In order to determine the true nature of these objects, HAADF STEM imaging was employed on several samples. This mode enables the user to obtain an image resulting predominantly from atomic number and specimen thickness contrast, unlike standard bright field TEM which primarily consists of atomic number, specimen thickness, and diffraction type contrast [32]. When using HAADF, regions containing relatively high atomic number material (electron dense) will appear light, while regions containing low atomic number elements will appear dark. Fig. 3 shows a HAADF STEM image of the LMW nanocomposite sample taken parallel to the ND axis. This image has a large number of round, disk-like, dark objects, thus verifying the

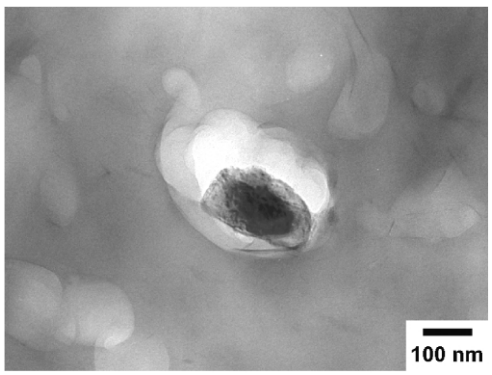

Fig. 4. TEM photomicrograph of platelet-pullout in LMW nylon 6 as a result of the microtoming process.

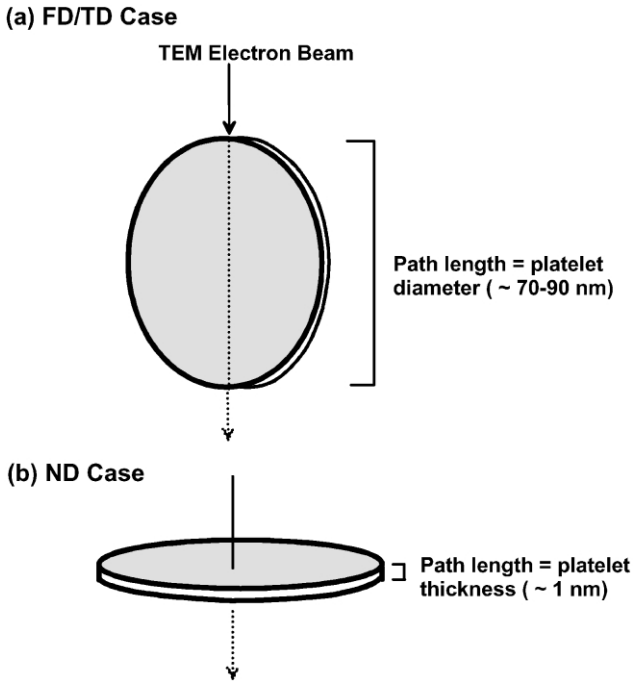

Fig. 5. Illustration of TEM electron beam–silicate platelet interactions encountered along the (a) flow or transverse and (b) the normal direction.

presence of void-like cavities which are believed to be a result of flake pullout; evidence of this is seen in Fig. 4. The photomicrograph shows a multi-layered stack that has been partially torn from the LMW polyamide matrix. Notably, the shape of the surrounding polymer matches that of the silicate stack.

The absence of dark platelet features in the TEM photomicrographs seen in Fig. 2(c) and (c′) needs to be addressed. Based on the observations made along the FD and TD axes in which platelets edges dominate, it is intuitive that the view parallel to the ND axis should contain a larger percentage of platelet faces. The absence of these faces can be explained by differences in silicate thickness that the transmission electron beam encounters along the three orthogonal directions. When the beam penetrates sections viewed parallel to the FD and TD axes, it predominantly encounters platelet edges. The relative thickness of the high atomic element containing platelets experienced by the beam is of the order of a platelet diameter, e.g. anywhere from (~30–200 nm. Fig. 5 shows this point. For the other extreme, i.e. views parallel to the ND axis, the electron beam travels through the face of dispersed platelets, whose thickness in the order of 1 nm (Fig. 5). This thickness is insufficient to yield any noticeable contrast. In addition, variation in thickness of the polymer matrix can often cloud transmitted features associated with platelet faces.

Based on these considerations, we conclude that both the HMW and the LMW based nanocomposites have a considerable number of void-like structures most likely caused by the microtoming process. The LMW composite

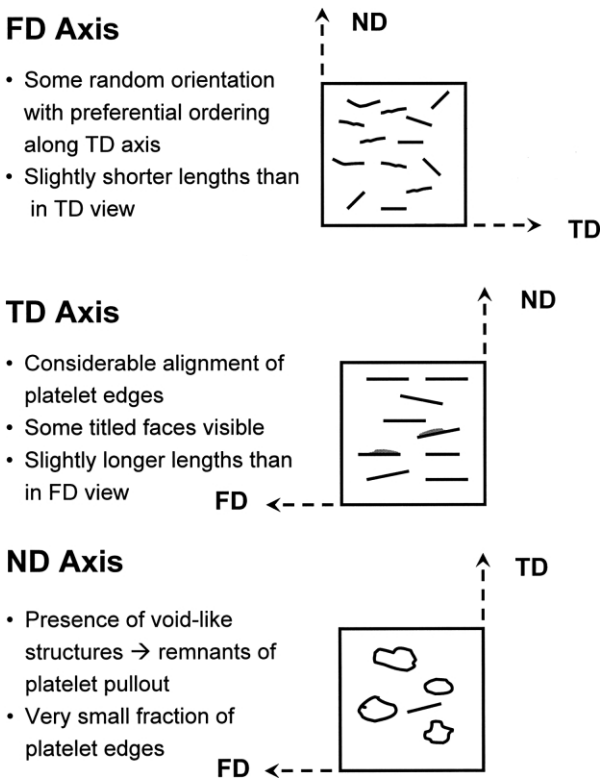

Fig. 6. Summary of orientation and anisotropy of silicate platelets along the three principle directions of injection-molded nylon 6 nanocomposites.

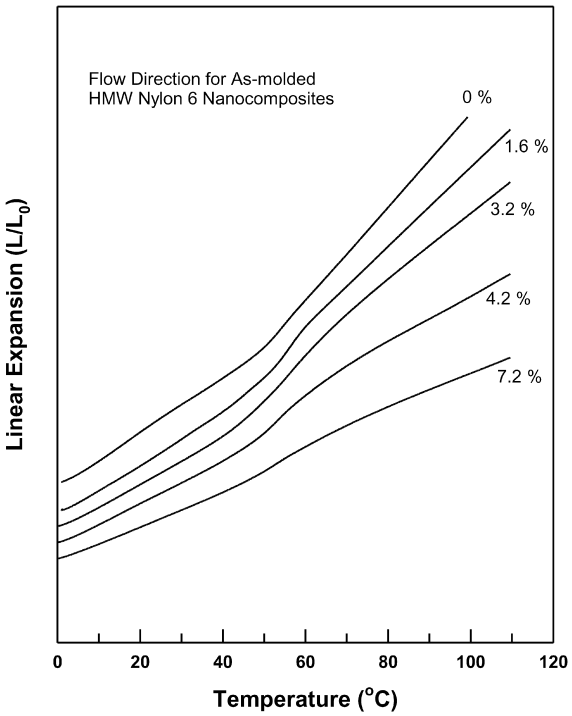

Fig. 7. Effect of MMT loading on linear thermal expansion of as-molded HMW nanocomposites in the FD.

does, however, contain a small fraction of platelet edges; this suggests incomplete alignment. Such misalignment again may stem from incomplete exfoliation of silicate platelets and/or lower levels of shear stress imparted by the less viscous polyamide matrix.

To address the possibility of silicate platelet dimensional anisotropy, in-plane TEM photomicrographs of HMW nanocomposites, taken parallel to the FD and TD axes, were analyzed using a semi-automated procedure as outlined in Section 2.4. The average platelet length viewed parallel to the FD axis was approximately 73 nm, while the length seen along the TD axis was approximately 91 nm. This anisotropy may help to explain the difference in alignment as seen in Fig. 2(a) and (b). An elliptical flake will orient such that the major axis aligns with the dominant flow field in which the shear stresses are the highest. In the case presented here, the polymer fills the mold along the FD; this will give rise to larger observed lengths when viewing parallel to the TD axis as compared to the FD axis. This type of behavior closely agrees with what has been reported for kaolinite platelets in Poiseuille flow regimes by Clarke et al. [26] as well as numerical simulations of platelet-like particles in simple shear flow regimes by Yamamoto and Matsuoka [27]. The latter researchers predicted that planar orientation of the particles should occur in the shear direction with the major axis of rectangular plates aligned in the direction of shear, which is what is seen here for montmorillonite disk-like platelets. The overall anisotropy and orientation aspects of silicate platelets seen within the central region of injection-molded specimens are summarized in Fig. 6.

5. Thermal expansion

5.1. As-molded nanocomposites

Fig. 7 shows the measured relative linear dimension (L/L_0) in FD as a function of temperature for as-molded HMW nylon 6 nanocomposites having various MMT contents. Linear thermal expansion coefficients below the nylon 6 glass transition temperature (T_g), α_g, and above T_g, α_r, were calculated from the slopes of the lines. As seen in Fig. 4, the as-molded specimens expand linearly from 0 to 40 °C and from 70 to 120 °C but non-linearly around the T_g (40 to 65 °C) due to relaxation effects during measurement [33]. The LECs for pure nylon 6 in the linear regions were found to be $\alpha_g = 8.5 \times 10^{-5}\ °C^{-1}$ and $\alpha_r = 14 \times 10^{-5}\ °C^{-1}$, which closely agree with reported data [15,33].

Fig. 8 shows the LECs above and below T_g in the flow (a) and transverse (b) directions for the as-molded HMW and LMW nylon 6 nanocomposites as a function of MMT content. Fig. 8(a) shows that α_r rapidly decreases as MMT loading increases for the HMW nylon 6 nanocomposites. For the pure nylon 6, α_r is almost twice as large as α_g. For the nanocomposite containing 6.5 wt% MMT, the value of α_r is almost identical with the value of α_g. It is interesting to note that the crossover of α_r and α_g occurs at a very low

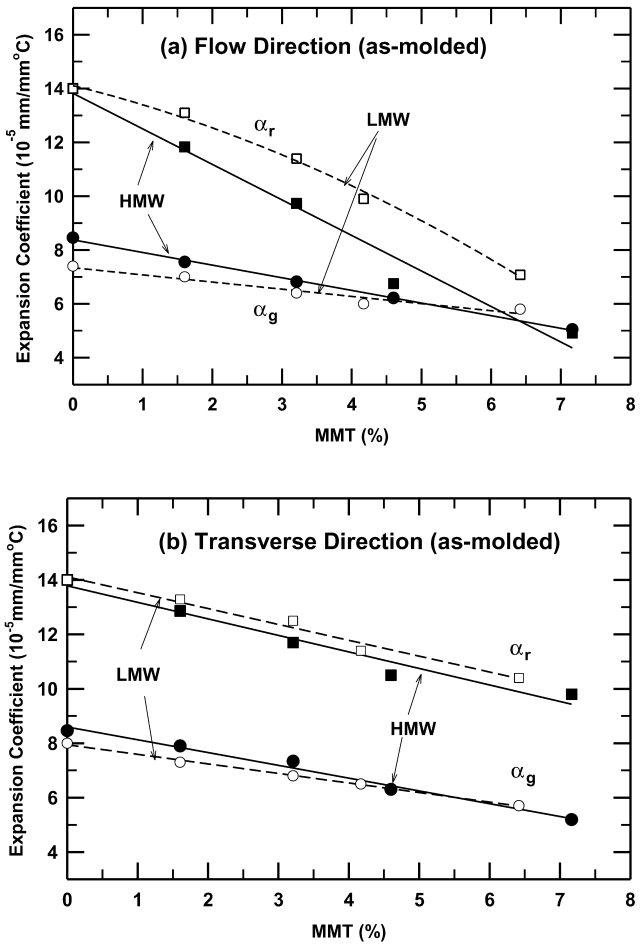

Fig. 8. Linear thermal expansion coefficient of as-molded specimens in the (a) flow and transverse (b) directions: (●) α_g for HMW, (○) α_g for LMW, (■) α_r for HMW, and (□) α_r for LMW nylon 6 nanocomposites.

filler loading compared to what is observed for conventional nylon 6 composites. For glass fiber composites, crossover occurs at approximately 20 wt% glass fiber [15]. The more effective reduction in thermal expansion for the nanocomposites is believed to stem from the nature of the filler, e.g. high modulus, high aspect ratio, two-dimensional reinforcement, and low CTE. Dispersion of individual silicate platelets provides a higher level of polymer constraint at much a lower filler concentration compared to conventional composites. The higher reduction in thermal expansion above the glass transition temperature is mainly due to the more extreme differences in stiffness and thermal expansion between the polymer matrix and the filler.

The LECs for the LMW nylon 6 nanocomposites are also shown in Fig. 8(a). Both α_g and α_r decrease with increasing MMT loading but not as rapidly for the nanocomposites based on LMW nylon 6 as those based on HMW nylon 6. This observation is not surprising due to the significant morphological differences seen earlier in the TEM photomicrographs. For a given MMT loading, the HMW nylon 6 nanocomposites have more exfoliated platelets than the LMW nylon 6 nanocomposites. Better exfoliation should lead to less thermal expansion during heating due to the larger number of platelets and higher aspect ratios that result from an increased amount of exposed silicate surface area in contact with the polymer. The larger constraining effect imposed by dispersed rigid platelets translates into lower thermal expansion coefficients.

Fig. 8(b) shows the LECs in TD for the as-molded HMW and LMW nylon 6 nanocomposites as a function of MMT concentration. The α_g for pure HMW nylon 6 is nearly the same in TD as in FD (Fig. 8(a)), indicating that injection-molded nylon 6 is nearly orthotropic. The α_r of nylon 6 in the TD specimens is slightly higher than that in the FD for the injection-molded specimens. This discrepancy may be attributed to differences in how the polymer chains orient within the injection-molded sample. Chains may have more orientation along FD than TD, thus leading to lower thermal expansion. Of course, disparity between the two directions may also reflect differences in the orientation of polymer crystallites. The nanocomposite α_r in TD, however, is significantly different from that in the FD (Fig. 8(a)). Both α_g and α_r in TD decrease as MMT is added. The values of α_g in the TD are not very different from those in the FD at a given MMT content. On the other hand, the decrease in α_r for the TD is not nearly as great as that in the FD, particularly for the HMW nylon 6 nanocomposites. This trend may be explained by platelet orientation and anisotropy effects. TEM photomicrographs presented earlier indicated a considerably higher degree of platelet alignment along FD than TD (Fig. 2(a′) and (a)). In addition, the average length of platelet edges were somewhat larger along the FD than the TD. Higher alignment and orientation of the major axis of the platelet along the direction of flow will lead to lower thermal expansion. It is not yet clear why the effects on nanocomposite thermal expansion caused by the nylon 6 molecular weight seem to be less in TD than in FD.

Fig. 9 shows plots of the linear thermal expansion coefficient in FD for as-molded LMW and HMW nanocomposites versus the Young's modulus in FD, measured at room temperature, normalized by the corresponding property of the matrix, α_m and E_m. The data for the thermal expansion are from Fig. 8(a) while the moduli are from a previous paper [9]. There is an excellent correlation between the relative linear thermal expansion coefficient and modulus. For either α_g or α_r, the data for the LMW and HMW nylon 6-based nanocomposites fall nearly on a single line indicating that the mechanisms controlling stiffness and linear thermal expansion coefficient have a similar origin.

5.2. Annealed nanocomposites

Fig. 10 shows the linear thermal expansion of annealed HMW nylon 6 nanocomposites. Comparison with Fig. 7 reveals that the relaxation processes in the vicinity of T_g during thermal expansion measurement are significantly reduced by annealing specimens at 150 °C for 8 h in a vacuum oven. The region of non-linear expansion for

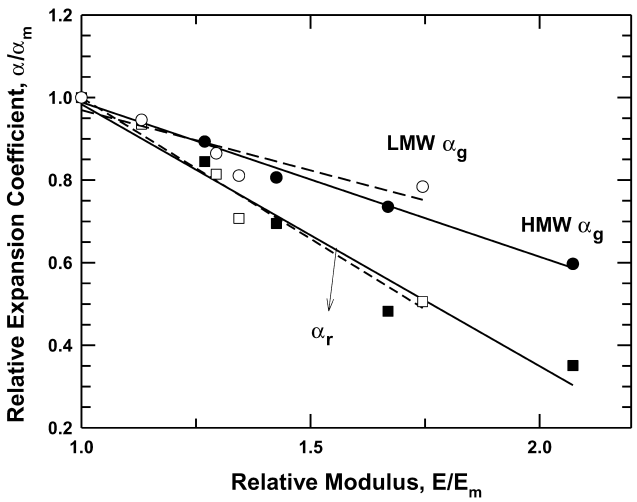

Fig. 9. Plots of relative linear thermal expansion coefficient versus relative modulus for as-molded specimens in the FD based on the data from α_g of HMW (●), α_g of LMW (○), α_r of HMW (■), and α_r of LMW (□) nylon 6 nanocomposites.

annealed specimens is limited to the temperature range from 40 to 60 °C.

Fig. 11 compares the measured thermal expansion in FD and TD for annealed HMW and LMW nanocomposites. The α_g and α_r of annealed HMW nanocomposites, as seen in Fig. 11(a), linearly decrease with MMT loading. However, the α_r of annealed samples shows a more moderate decrease compared to as-molded samples. A similar pattern is observed for the nanocomposites based on LMW nylon 6.

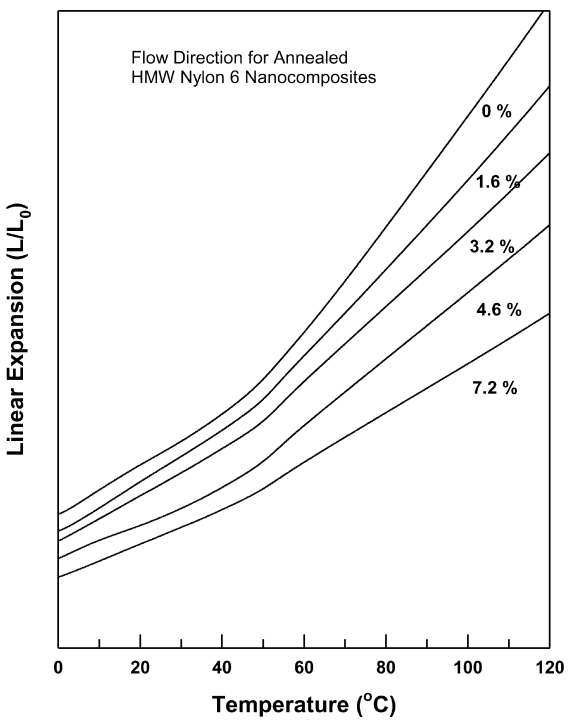

Fig. 10. Effect of MMT loading on linear thermal expansion of annealed HMW nylon 6 nanocomposites in the FD.

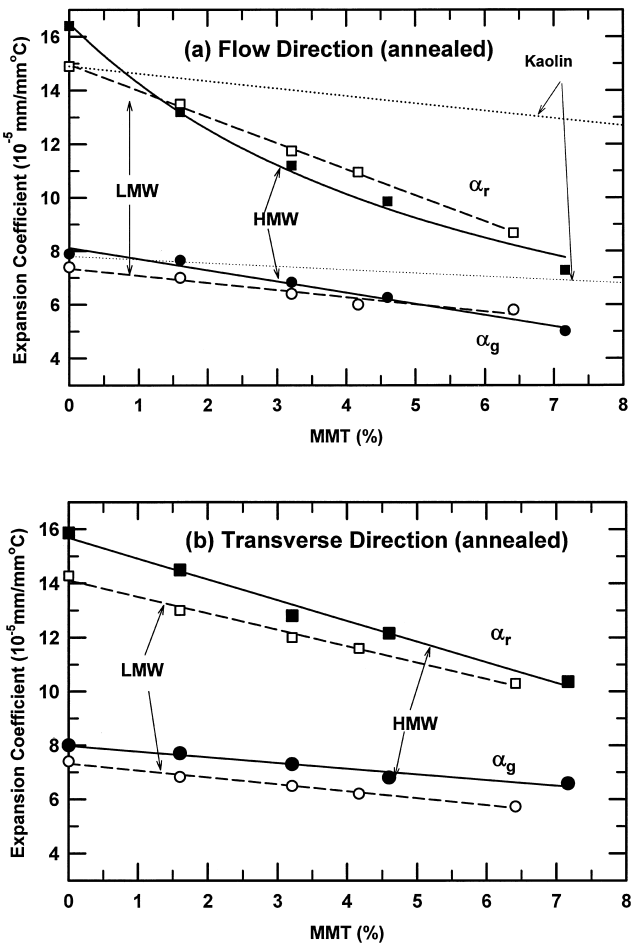

Fig. 11. Linear thermal expansion coefficients of annealed specimens (a) in the flow and (b) in the transverse directions: (●) α_g for HMW, (○) α_g for LMW, (■) α_r for HMW, and (□) α_r for LMW nylon 6 nanocomposites. Dotted lines in part (a) are for kaolin from Ref. [15].

Several factors may contribute to the differences between as-molded and annealed specimens. For example, annealing could cause some loss of orientation of the platelets owing to the relaxation of taut nylon 6 molecules developed during injection molding or the greater relaxation of as-molded samples during measurement may reduce the amount of observed thermal expansion. Differences in the crystalline properties of the polymer matrix may also contribute to changes in the thermal expansion behavior between the as-molded and annealed specimens.

Fig. 11(b) shows the thermal expansion in the TD for annealed HMW and LMW nanocomposites as a function of MMT concentration. The LMW nanocomposites show slightly lower levels of thermal expansion than the HMW nanocomposites. This stems primarily from differences in the thermal expansion behavior of the pure LMW and HMW nylon 6 matrices (compare the values of expansion coefficient at 0% MMT). Annealing of HMW nylon 6 causes a noticeable increase in α_r for both FD and TD; annealing has less effect on α_r for LMW nylon 6. The differences between LMW and HMW nylon 6 may arise

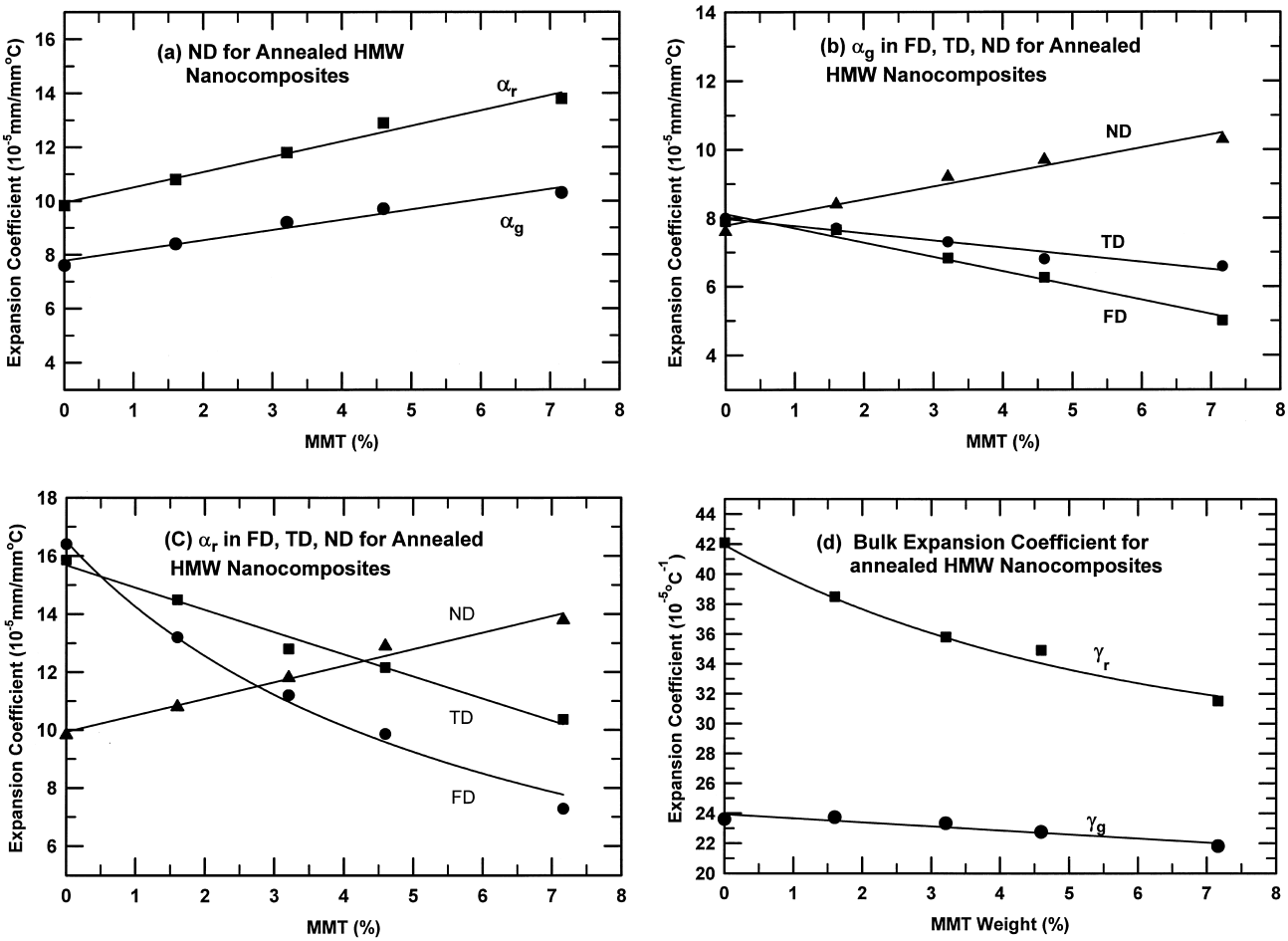

Fig. 12. (a) Linear thermal expansion coefficients in the ND, (b) comparisons of α_g in all three directions, (c) comparisons of α_r in all three directions, and (d) bulk thermal expansion coefficient for annealed HMW nylon 6 nanocomposites.

from the effect of molecular weight on crystallization. However, a more detailed study involving techniques like wide angle X-ray diffraction and/or differential scanning calorimetry would be needed to explain in-depth the cause for these differences in behavior of the two matrices; this is beyond the scope of the current study. Comparison of Fig. 11(a) and (b) shows that α_g in TD is higher than that in FD as can also be observed in Fig. 8(a) and (b).

The dotted lines in Fig. 11(a) represent results from Segal [15] for kaolin/nylon 6 composites. Both the HMW and the LMW nylon 6-based nanocomposites show better efficiency in reduction of linear thermal expansion coefficients than these kaolin composites based on a medium molecular weight [MMW] nylon 6 [9]: i.e. the slopes of thermal expansion coefficient versus MMT loading stand in the order: HMW nylon 6-based nanocomposite > LMW nylon 6-based nanocomposite > MMW nylon 6-based kaolin composite. Thus, the nanocomposites offer superior dimensional stability at low filler content (lower material density or weight) compared to conventional composites.

For the annealed HMW nanocomposites, the linear thermal expansion coefficient was also measured in ND, which allows a more detailed comparison of the anisotropy of thermal expansion and computation of bulk expansion coefficients for the nanocomposites. Fig. 12(a) shows α_g and α_r in the ND while Fig. 12(b) and (c) compare the α_g and α_r, respectively, in the FD, TD, and ND. Fig. 12(d) shows the bulk expansion coefficient γ, calculated by adding the linear coefficients in the three directions, i.e. $\gamma = \sum_{i=1}^{3} \alpha_i$.

The thermal expansion coefficient in ND increases with increasing MMT loading due to a 'squeezing' effect [20]. In the TD and FD, the polymer is highly constrained which creates a squeezing force exerted in the ND, thus resulting in increased expansion. The bulk expansion coefficients is less sensitive to the MMT loading, as seen in Fig. 12(d), than the linear thermal expansion coefficients in the FD and TD, as seen in Fig. 12(b) and (c).

The data in Figs. 8, 11, and 12 are summarized in Table 3 to facilitate more detailed comparisons. The thermal expansion coefficients for pure nylon 6 show significantly less dependence on specimen direction than observed for the nanocomposites. For annealed HMW nylon 6, the α_g in the ND is slightly lower than in the FD and TD; the latter are almost identical. On the other hand, α_g for LMW nylon 6 shows more anisotropy and opposite trends for the as-molded and annealed specimens: α_g (TD) > α_g (FD) for

Table 3
Linear thermal expansion coefficients (in units of 10^{-5} mm/mm °C) for nylon 6-$(HE)_2M_1R_1$ nanocomposites

MMT (wt%)	As-molded				Annealed					
	Flow		Transverse		Flow		Transverse		Normal	
	α_g	α_r	α_g	α_r	α_g	α_r	α_g	α_r	α_g	α_r
Matrix = HMW nylon 6										
0	8.5	14.0	8.4	14.0	7.9	16.4	8.0	15.9	7.7	9.8
1.6	7.6	11.8	7.9	12.9	7.6	13.2	7.7	14.5	8.4	10.8
3.2	6.8	9.7	7.3	11.7	6.8	11.2	7.3	12.8	9.2	11.8
4.6	6.2	6.8	6.3	10.5	6.3	9.9	6.8	12.2	9.7	12.9
7.2	5.1	4.9	5.2	9.8	5.0	7.3	6.5	10.4	10.3	13.8
Matrix = LMW nylon 6										
0	7.4	14.0	8.0	14.0	8.0	14.9	7.4	14.3		
1.6	7.0	13.1	7.3	13.3	7.0	13.5	6.8	13.0		
3.2	6.4	11.4	6.8	12.5	6.3	11.8	6.5	12.0		
4.2	6.0	9.9	6.5	11.4	6.0	11.0	6.2	11.6		
6.4	5.8	7.1	5.7	10.4	5.7	8.7	5.7	10.3		

as-molded specimens while α_g (FD) > α_g (TD) for annealed specimens. The difference in the LMW and HMW nylon 6 materials may relate to issues of crystallization, rheology, and how the two couple during processing. The nanocomposites show a high degree of anisotropy in thermal expansion behavior, particularly above T_g.

The efficiency of the clay for reducing the linear coefficient of thermal expansion can be represented by the derivative dα/d*MMT%*. Table 4 shows the derivatives deduced from Figs. 8 and 11. In the region above T_g, the clay gives a greater reinforcement effect in the region above T_g than below primarily due to the larger difference in the mechanical properties of the matrix and the filler in this region. The nylon 6 modulus drops significantly when heated above T_g while the clay particles remain very rigid.

6. Modeling

The dependence of the thermal expansion behavior of polymer composites on various filler characteristics, e.g. type, shape, concentration, etc. has been discussed for decades [18,20–23]. A limited number of models have been developed to describe how fillers affect thermal expansion behavior. Chow developed a model capable of predicting the linear thermal expansion of composites containing anisotropic particles which will be used here since it appears to be both applicable for current purposes and relatively simple to use. The following discussion employs the nomenclature used by Chow [18]. In this model, fillers are considered as identical spheroids whose the corresponding axes are perfectly aligned in the composite

$$(x_1^2 + x_2^2)/a^2 + x_3^2/c^2 = 1 \quad (1)$$

The anisotropic shape is characterized by the ratio of the major to the minor axes $\rho = c/a$ of the spheroid; three special shapes along with their respective ρ are depicted in Fig. 13. For a composite comprised of perfectly aligned ellipsoidal particles embedded in a matrix, the longitudinal thermal expansion coefficient (α_L), i.e. in the direction parallel to the major axis of the particle is given by

$$\alpha_L = \alpha_m + \frac{k_f}{k_m}\frac{(\gamma_f - \gamma_m)G_1\phi}{2K_1G_3 + G_1K_3} \quad (2)$$

while the transverse thermal expansion coefficient (α_T) is given by

$$\alpha_T = \alpha_m + \frac{k_f}{k_m}\frac{(\gamma_f - \gamma_m)G_3\phi}{2K_1G_3 + G_1K_3} \quad (3)$$

where k_f and k_m refer to the bulk modulus for the filler and

Table 4
Derivative of the thermal expansion coefficients versus MMT loading level (dα/dMMT% in units of 10^{-5} mm/mm °C)

	As-molded				Annealed					
	Flow		Transverse		Flow		Transverse		Normal	
	α_g	α_r	α_g	α_r	α_g	α_r	α_g	α_r	α_g	α_r
HMW	−0.47	−1.32	−0.47	−0.61	−0.42	−1.23	−0.21	−0.77	0.38	0.57
LMW	−0.27	−1.10	−0.35	−0.58	−0.32	−0.97	−0.26	−0.61	–	–

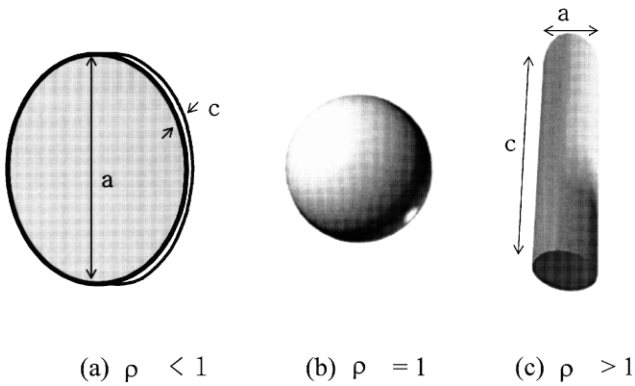

Fig. 13. Illustrations of particle shapes in relation to the Chow model parameter, $\rho = c/a$: (a) disk, (b) spheroid, and (c) fiber.

matrix while γ_f and γ_m are bulk thermal expansion coefficients, respectively. The bulk and shear moduli, k and μ, are used to calculate K_i and G_i functions [19]

$$K_i = 1 + \left(\frac{k_f}{k_m} - 1\right)[(1-\phi)\alpha_i + \phi] \quad (4)$$

$$G_i = 1 + \left(\frac{\mu_f}{\mu_m} - 1\right)[(1-\phi)\beta_i + \phi] \quad (5)$$

where α_i and β_i are functions of ρ and Poisson's ratio of the matrix. In using this model, the c-axis is assumed parallel to the FD; thus, Eqs. (2) and (3) can be used to model fibers and disks aligned along the FD, respectively.

Fig. 14 shows the effect of low concentrations of aligned disks on the thermal expansion coefficient in the FD calculated from Eq. (3) for various aspect ratios, $A_f = 1/\rho$. The calculated curves were based on the following parameters: $E_f = 172.0$ GPa [30,34,35], $E_{m(HMW)} = 2.75 \times$ GPa [9], $E_{m(LMW)} = 2.82$ GPa [9], a matrix Poisson ratio = 0.33 [15], a filler Poisson ratio = 0.20 [21], $\gamma_f = 0.5 \times 10^{-5}\ ^\circ C^{-1}$ [36], and γ_m was calculated from experimental data for pure nylon 6 using $\gamma = \Sigma\alpha_i$. Bulk and shear moduli for isotropic materials are interrelated by $k = E/2(1+\nu)$ and $\mu = E/(3-2\nu)$, respectively [21]. McKinstry [36] has shown that the linear thermal expansion coefficients within the layer for several clay minerals range from 3.5 to $6.9 \times 10^{-6}\ ^\circ C^{-1}$. The linear thermal expansion coefficient for montmorillonite, α_f, is estimated by averaging the data of six different clays including muscovite, kaolinite, talc, etc. In this reference, the thermal expansion coefficient within the layer for bulk clays is different from that perpendicular to the layer. However, the thermal expansion coefficient within the layer may better represent that for a single platelet since the thermal expansion coefficient perpendicular to the layer counts gallery expansion as well. Thus, we take γ_f as three times the in-plane LEC. Note that parameters are based on the properties below T_g. The points are the experimental data for as-molded HMW nanocomposites in the FD. Fig. 14(b) shows the corresponding experimental and theoretical comparisons for nanocomposites based on LMW nylon 6. If we

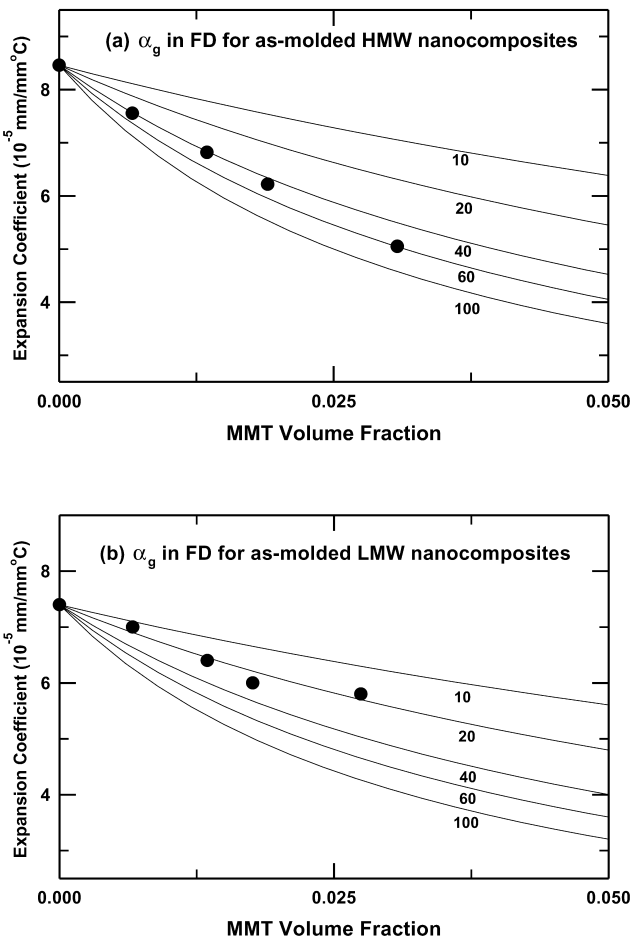

Fig. 14. Comparisons of theoretical linear thermal expansion coefficients for different aspect ratios in the FD for as-molded (a) HMW and (b) LMW nylon 6 nanocomposites with experimental data.

assume that the particles are perfectly aligned in the FD for these nanocomposites, then the theory suggests the aspect ratios in the FD are approximately $A_f = 50$ and 20 for HMW and LMW based nanocomposites, respectively.

Fig. 15 compares the measured α_g in the FD, TD, and ND for annealed, injection-molded HMW nylon 6 nanocomposites with the predictions of the Chow theory. The experimental data seem to match the theoretical curves for $A_f \sim 15$ in the TD and $A_f \sim 60$ in the ND. The data for the FD do not fall along the line for any single aspect ratio curve, but is consistent with $A_f \sim 40$ at the highest loading. It is unclear why such behavior exists only in this direction and not the others. The fact that the same aspect ratio is not obtained in each comparison supports the TEM observations that the platelets are not circular nor perfectly aligned along the FD and TD.

Fig. 16 compares bulk expansion coefficients above and below T_g obtained experimentally, viz. the annealed HMW nylon 6 nanocomposites, and theoretically. Experimental bulk expansion values were obtained by summing the individual CTEs for the three principle directions. Likewise,

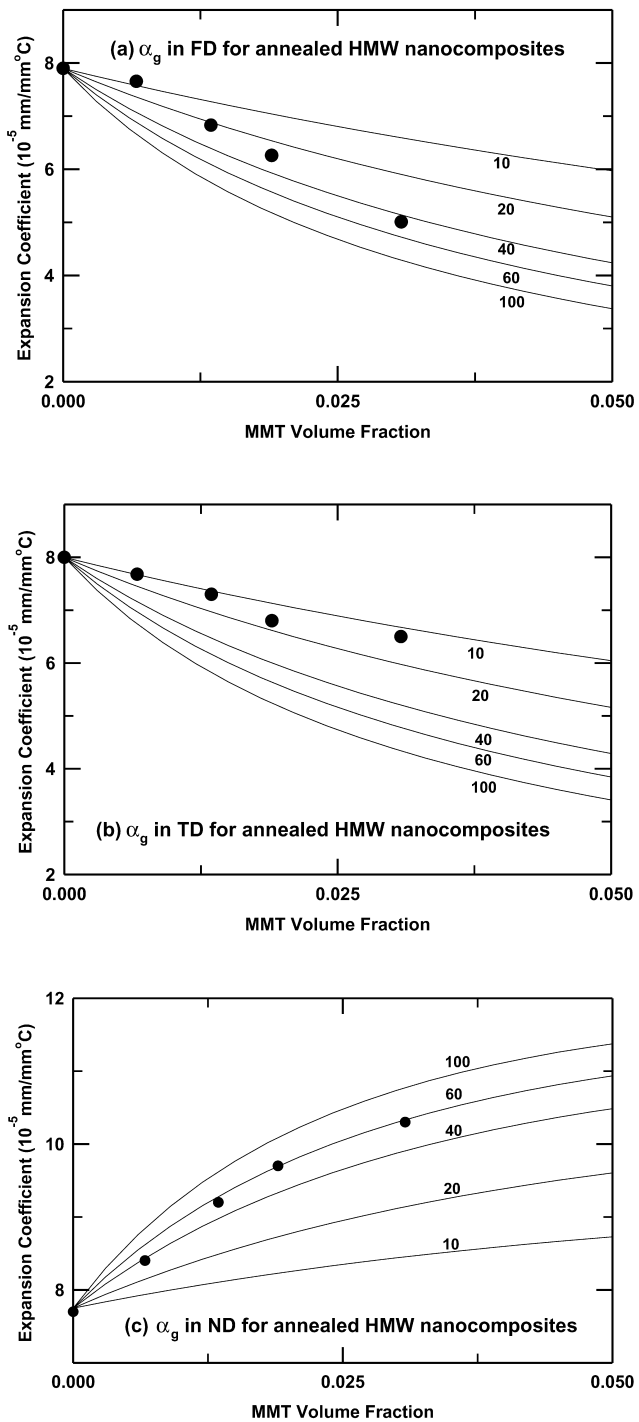

Fig. 15. Comparisons of theoretical linear thermal expansion coefficients for different aspect ratios in the (a) flow, (b) transverse, and (c) normal directions for annealed HMW nylon 6 nanocomposites with experimental data.

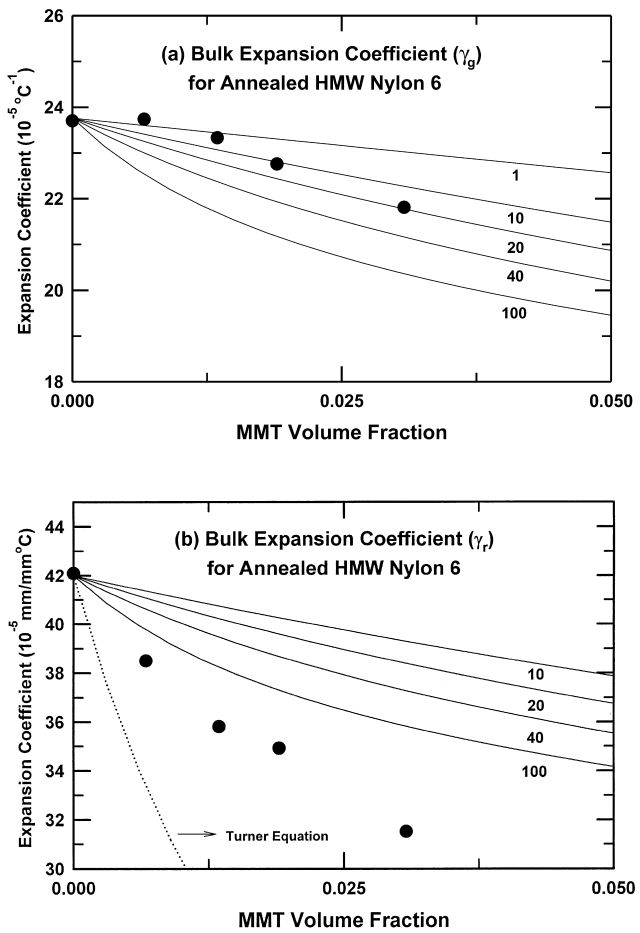

Fig. 16. Comparisons of bulk thermal expansion coefficients predicted by the Chow model for various platelet aspect ratios with experimental values below T_g, see γ_g in part (a), and above T_g, see γ_r in part (b), for annealed HMW nylon 6 nanocomposites. Dotted line in part (b) represents the Turner equation.

the predicted bulk coefficients were calculated using a constant aspect ratio for each direction. The reader should be reminded that both the experimental data and the theoretical predictions show the LEC to decrease as clay is added in the FD and the TD and to increase in the ND. Fig. 16(a) shows a relatively small effect on the bulk expansion coefficient by adding montmorillonite to HMW nylon 6, e.g. less than a 10% decrease in γ_g for the highest MMT concentration. The Chow model does not fit the data very well for any fixed aspect ratio; however, one should not attach much significance to this since the difference is likely within the experimental error. The key point in Fig. 16(a) is that both the model and the data show only a small decrease in γ_g.

On the other hand, the experimental data for bulk expansion in the rubbery region (Fig. 16(a)) reveals a much steeper decrease in the thermal expansion with respect to MMT content, as much as 25%, compared to the glassy region data. The larger drop seen in Fig. 16(b) arises from the extreme differences in stiffness and thermal expansion between the filler and the matrix. Of course, the differences in these properties are somewhat smaller below the T_g of nylon 6. Unlike the experimental data in the glassy region, the data in the rubbery region fall well below the predictions of the Chow model for any realistic aspect ratio. Interestingly, the data are underestimated by the predictions of the

Table 5
Aspect ratios ($A_f = 1/\rho = a/c$) of clay particles obtained by comparing experimental α_g data to the Chow model

	As-molded		Annealed		
	FD	TD	FD	TD	ND
HMW	50	20–60	40	15	60
LMW	30	40	20	25	–

Turner equation [22]

$$\gamma = \frac{\gamma_m \phi_m k_m + \gamma_f \phi_f k_f}{\phi_m k_m + \phi_f k_f} \quad (6)$$

which represents a lower bound for thermal expansion.

There are a number of reasons why the Chow model inadequately describes the experimental data. First, the model assumes that the particles are perfectly aligned which clearly is not the case here as seen by TEM. Slight deviations from perfect alignment can result in a significant diminution of the restraint on the thermal expansion; note that the thermal expansion actually increases with clay content normal to the platelet direction (ND). Second, the model assumes a monodispersed distribution of platelet diameters and stack thicknesses, i.e. aspect ratio, while in fact there is a distribution of both. Third, the model assumes that the matrix is isotropic, while nylon 6 is a semi-crystalline polymer consisting of two phases with varying degrees of orientation that may be affected by the presence of the clay platelets. Variations in crystalline form, size, shape, and quantity, may have a significant effect on thermal expansion. In addition, crystalline properties are also sensitive to thermal treatment, e.g. annealing. Finally, there are variety of additional issues that might affect the goodness of fit of the model to the data; we have assumed that the modulus of the matrix is constant from 0 to 40 °C and 70 to 120 °C and that the organic modifier on the clay has no effect on expansion behavior. Ultimately, to best test the predictive capability of the Chow model requires a completely amorphous polymer in which the clay platelets can be easily dispersed and highly aligned in one direction.

The aspect ratios of clay particles in the nanocomposites based on HMW and LMW nylon 6 deduced by comparison with the theoretical calculations are summarized in Table 5. The estimated aspect ratios for LMW nylon 6 nanocomposites are almost identical in the FD and TD while those for annealed HMW nylon 6 nanocomposites in the two directions are quite different, A_f (FD) $\gg A_f$ (TD). This could be anticipated from the TEM analysis given earlier; LMW nanocomposites show relatively small differences in orientation along the flow or TD while HMW nanocomposites show preferential alignment along the FD but poor orientation along the TD.

7. Conclusion

The reduction in linear thermal expansion coefficients caused by adding clay platelets to nylon 6 nanocomposites prepared by melt blending was found to be very efficient compared to conventional composites. The thermal expansion coefficients of nanocomposites formed from a HMW nylon 6 were lower than those formed from a LMW nylon 6. The enhanced behavior for the HMW nylon 6 nanocomposites was attributed to a higher degree of exfoliation, higher aspect ratio, and higher degree of orientation.

The thermal expansion coefficient in the FD of injection-molded specimens was observed to be significantly lower than in the TD. This trend is attributed to a lower degree of alignment of the exfoliated platelets, as indicated by TEM photomicrographs, in the TD compared to the FD. Small changes from perfect planar orientation result in significant changes in thermal expansion behavior. Some of the observed differences in the FD and TD may also be attributed to anisotropy of the clay platelets; there is some evidence that the platelets may be more elliptical shape rather than simple circular disks.

A model developed by Chow was used to estimate aspect ratios of exfoliated particles. The model indicates that the aspect ratio of the particles in the HMW nylon 6 nanocomposites is around 50 as compared to 20 in the LMW nylon 6 nanocomposites. This comparison assumes perfect alignment of the platelets; thus, the actual aspect ratio may be higher than the model suggests. The imperfect orientation or anisotropic platelet shape is also seen in the different aspect ratios when the theory is compared with data in the three different coordinate directions. It appears that the model might be useful for prediction of thermal expansion behavior if a perfect nanocomposite morphology (i.e. platelet orientation) could be obtained during processing and accurately characterized by TEM.

Acknowledgements

This work was supported by the Texas Advanced Technology Program under grant number 003658-0067 and by the Air Force Office of Scientific Research. The authors would like to thank Southern Clay Products, Inc. for providing clay materials and technical assistance and Dr Chaunbin Mao for his assistance with STEM imaging.

References

[1] Usuki A, Koiwai A, Kojima Y, Kawasumi M, Okada A, Kurauchi T, Kamigaito O. J Appl Polym Sci 1995;55:119–23.
[2] Wang Z, Pinnavaia TJ. Chem Mater 1998;10:3769–71.
[3] Messersmith PB, Giannelis EP. J Polym Sci, Part A: Polym Chem 1995;33:1047–57.
[4] Yano K, Usuki A, Okada A, Kurauchi T, Kamigaito O. J Polym Sci, Part A: Polym Chem 1993;31:2493–8.

[5] Liu L, Qi Z, Zhu X. J Appl Polym Sci 1999;71:1133–8.
[6] Gu A, Chang F-C. J Appl Polym Sci 2001;79:289–94.
[7] Cho JW, Paul DR. Polymer 2001;42(3):1083–94.
[8] Dennis HR, Hunter DL, Chang D, Kim S, White JL, Cho JW, Paul DR. Polymer 2001;42:9513–22.
[9] Fornes TD, Yoon PJ, Keskkula H, Paul DR. Polymer 2001;42: 9929–40.
[10] Fornes TD, Yoon PJ, Keskkula H, Paul DR. Polymer 2002;43: 2121–2.
[11] Usuki A, Kojima Y, Kawasumi M, Okada A, Fukushima Y, Kurauchi T, Kamigaito O. J Mater Res 1993;8(5):1179–84.
[12] Carrado KA, Xu L. Chem Mater 1998;10:1440–5.
[13] Garces JM, Moll DJ, Bicerano J, Fibiger R, McLeod DG. Adv Mater 2000;12:1835–9.
[14] Mod Plast 2001:10;37.
[15] Segal R. Polym Engng Sci 1979;19:365–72.
[16] Okada A, Kawasumi M, Usuki A. Mater Res Soc Symp Proc 1990; 171:45–50.
[17] Okada A, Usuki A. Mater Sci Engng 1995;C3:109–15.
[18] Chow TS. J Polym Sci, Polym Phys 1978;16:967–70.
[19] Chow TS. J Polym Sci, Polym Phys 1978;16:959–65.
[20] Ashton JF, Halpin JC, Petit PH. Structure property relationship for composite materials. Primer composite materials analysis. Lancaster: Technomic; 1969. Chapter 5.
[21] Schapery RA. J Comp Mater 1968;2:380–404.
[22] Holliday L, Robinson J. J Mater Sci 1973;8:301–11.
[23] Feltham SJ, Yates B, Martin RJ. J Mater Sci 1982;17:2309–23.
[24] Kojima Y, Usuki A, Kawasumi M, Okada O, Fukushima Y, Kurachi T, Kamigaito O. J Mater Res 1993;8:1185–9.
[25] Lincoln DM, Vaia RA, Wang Z, Hsiao BS, Krishnamoorti R. Polymer 2001;42:9975–85.
[26] Clarke SM, Rennie AR, Convert P. Europhys Lett 1996;35:233–8.
[27] Yamamoto S, Matsuoka T. J Chem Phys 1997;107:3300–8.
[28] Schmidt G, Nakatani AI, Han CC. Rheol Acta 2002;41:45–54.
[29] Brune DA, Bicerano J. Polymer 2002;43:369–87.
[30] Lusis J, Woodhams BT, Xanthos M. Polym Engng Sci 1973;13: 139–45.
[31] Oshinski AJ, Keskkula H, Paul DR. Polymer 1996;37(22):4891–907.
[32] Williams DB, Carter CB, Transmission electron microscopy, vols. 1–4. New York: Plenum Press; 1996.
[33] Kohan MI, Nylon plastics handbook. New York: Hanser; 1995.
[34] van Es M, Xiqiao F, van Turnhout J, van der Giessen E. In: Al-Malaika S, Golovoy A, Wilkie CA, editors. Comparing polymer–clay nanocomposites with conventional composites using composite modeling. Specialty polymer additives. Oxford: Blackwell; 2001. Chapter 21.
[35] Utracki LA, Vu Khanh T. In: Miles IS, Rostami S, editors. Filled polymers. Multicomponent polymer systems. Essex: Longman; 1992. Chapter 7.
[36] McKinstry HA. Am Mineral 1965;50:212–22.